ACOUSTICS 2012

Simulation of wave propagation in anisotropic poroelastic bone plate immersed in fluid

V.-H. Nguyen and S. Naili

Université Paris-Est, 61 avenue du Général de Gaulle, 94010 Créteil Cedex, France
vu-hieu.nguyen@univ-paris-est.fr

This paper deals with modeling of the ultrasound axial transmission technique for *in vivo* cortical long bone which is known as being a anisotropic solid medium with functionally graded porosity. The bone is modeled as an anisotropic poroelastic medium using the Biot's theory. We develop a hybrid spectral/finite element formulation to obtain the time-domain solution of ultrasonic waves propagating in a poroelastic plate immersed two fluid halfspaces. The numerical method is based on a combined Laplace-Fourier transform which solves the problem in the frequency-wavenumber domain. In the spectral domain, as radiation conditions may be exactly introduced in the infinite fluid halfspaces, only the heterogeneous solid layer needs to be analyzed using finite element method. Several numerical tests are presented showing very good performances of the proposed approach. A preliminary study on the FAS (First Arrived Signal) velocities computed by using equivalent elastic and poroelastic models will be presented.

1 Introduction

In recent years, quantitative ultrasound (QUS) techniques for assessing the properties of bone have received much attention due to its potential in estimating bone fragility and/or fracture risk. For measuring *in vivo* material properties of cortical long bones, a so-called "axial transmission" (AT) technique has been developed [1]. The AT technique uses a set of ultrasonic transducers (transmitters and receivers) linearly placed in the same side of the investigated skeletal site along a direction close to the long bone axis. The transmitter emits an ultrasound pulse wave (around 250 KHz-2 MHz) that propagates along the cortical layer of bones. The analysis of the signals received at the receivers serve for estimating the geometrical parameters as well as mechanical characteristics of the cortical bone at the measured skeletal site.

Mechanical modeling of this experiment deals with describing a vibro-acoustic problem of a solid waveguide (which represents cortical bone) coupled with two fluid media (which represents soft tissues such as skin or marrow). Assessment of the bone's material properties requires careful analysis of the reflections, conversion modes and interferences of waves within the bone structure. However, current development of ultrasound techniques is still limited since the interaction between ultrasound and bone remains poorly understood due to the complex nature of bone which has a porous microstructure spanning many length scales.

From the point of view of mechanics, cortical bone is a heterogeneous, anisotropic and porous material. At the macroscopic scale, porosity in the radial direction (defined in the bone's cross-section plan) is heterogeneous. As the macroscopic mechanical properties of bone have been shown to strongly depend on its porosity [2], cortical bone may naturally be considered as a functionally graded material.

Many of the past studies have focused on the modeling of guided waves in long bones by using fluid-loaded homogeneous/multilayer/functional graded plate models. The understanding of wave phenomena involved in multilayer structures has been studied by many authors in the frequency-domain [3] or in the time-domain [4, 5]. In these studies, the cortical bone material has been considered as an equivalent (visco-)elastic medium of which the effective macroscopic mass density and effective macroscopic elasticity tensor are estimated from its porosity. The presence of the interstitial fluid, which was considered in many works for the analysis of the behavior of cortical bone tissue under low frequency loading (*e.g.* [6, 7]) or of ultrasonic wave propagation through cancellous bones (*e.g.* [8, 9]), has usually been neglected when studying ultrasonic wave propagation in cortical bones.

In order to solve the time-domain wave propagation problem in the multilayer structures, there are mainly two approaches. The first one involves using (semi-)analytical methods (*e.g.* [10]). The second one involves using numerical methods such as the finite difference method (FDM) [4] or the finite element method (FEM) [11]. Numerical methods are often more efficient to treat problems with inhomogeneous materials or complex geometries. However, most numerical methods require important computational costs, especially for problems in the high-frequency domain. Moreover, absorbing boundary conditions are required for considering unbounded domains [4, 11]. Alternatively, when considering waveguides with constant geometrical and mechanical properties along one direction, semi-analytical/finite element techniques have been employed (see *e.g.* [12, 13, 14]).

This paper presents a numerical procedure to simulate the ultrasonic wave propagation in bone plate immersed in fluid. The bone plate is not modeled as an equivalent elastic medium but as a functionally-graded anisotropic poroelastic medium. The numerical method is based on the hybrid semi-analytical/finite element technique. The key point of this method consists in using a hybrid algorithm which begins by employing the Laplace-Fourier transform (with respect to time and to the longitudinal direction of the waveguide) to transform problem into the frequency-wavenumber domain. Then, the wave equations in the spectral domain governed in 1D cross-section domain, which may actually have inhomogeneous material properties, can be easily handled using the finite element method [5, 14, 15].

This paper is organized as follows. Section 2 presents the governing equations of an anisotropic poroelastic bone plate immersed in fluid. Next, sections 3 presents the problem governed in Laplace-Fourier domain and the finite element formulation in this domain. Then, some numerical tests are presented in Section 4 to validate the proposed procedure. We will also present some comparison of the FAS (First Arrived Signal) velocities computed by using equivalent elastic and poroelastic models. Finally, conclusion and discussion will be presented in Section 5.

2 Description of the problem

2.1 Geometrical configuration

In this work, we will employ a two dimensional (2D) configuration which has been shown to be an appropriate geometrical model for describing the ultrasound wave in long bone in the framework of the AT technique [4]. Let $\mathbf{R}(\mathrm{O};\mathbf{e}_1,\mathbf{e}_2)$ be the reference Cartesian frame. We denote

the coordinates of a point $\boldsymbol{x}$ in $\mathbf{R}$ by (x_1, x_2) and the time by t. The fluid occupies both half-spaces Ω_1^f and Ω_2^f. The bone layer occupies the unbounded domain Ω^b. Two plane interfaces between the bone layer Ω^b and the fluid domains Ω_1^f and Ω_2^f are respectively denoted by Γ_1^{bf} and Γ_2^{bf} (Fig. 1). The bone plate's thickness is denoted by h.

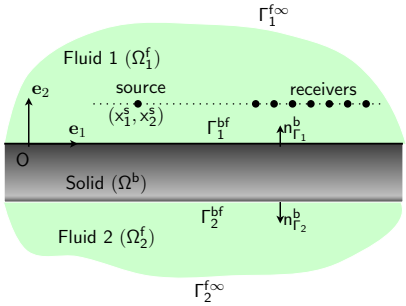

Figure 1: The trilayer model of axial transmission test

2.2 Governing equations

Wave equation in fluid domains The fluids occupying the domains Ω_1^f and Ω_2^f are modeled by linear acoustic fluids. Their mass densities and bulk modulus are denotes by ρ_1, K_1 and ρ_2, K_2, respectively. The acoustical source is located in the upper fluid domain Ω_1^f. In later domain, the linear acoustic wave equation may be expressed only in terms of the pressure field $p_1(\boldsymbol{x}, t)$ as follows:

$$\ddot{p}_1 - c_1^2 \Delta p_1 = \rho_1 c_1^2 F(t)\, \delta(x_1)\delta(x_2 - x_2^s), \quad \forall \boldsymbol{x} \in \Omega_1^f, \qquad (1)$$

where c_1 is the wave celerity in Ω_1^f which is defined by: $c_1 = \sqrt{K_1/\rho_1}$; $F(t)$ is a scalar function and $\delta(.)$ is Dirac's delta function. Similarly, the pressure field $p_2(\boldsymbol{x}, t)$ in the fluid domain Ω_2^f verifies:

$$\ddot{p}_2 - c_2^2 \Delta p_2 = 0, \quad \forall\, \boldsymbol{x} \in \Omega_2^f. \qquad (2)$$

Dynamic equations of anisotropic porous layer The bone material is assumed to consist of a solid skeleton (with mass density ρ_s) and a connected pore network saturated by fluid (with mass density ρ_f). Here, the anisotropic poroelasticity theory [16] is used to describe the dynamic behavior of bone layer. Neglecting the body forces (other than inertia), the equations of wave propagation within the bone layer read:

$$\rho\, \ddot{\boldsymbol{u}}^s + \rho_f \ddot{\boldsymbol{w}} - \mathbb{L}^T \boldsymbol{s} = \mathbf{0}, \qquad (3)$$

$$\rho_f \ddot{\boldsymbol{u}}^s + \boldsymbol{k}^{-1}\dot{\boldsymbol{w}} + \boldsymbol{b}\ddot{\boldsymbol{w}} + \mathbb{L}^T \boldsymbol{m} p = \mathbf{0}, \qquad (4)$$

where $\rho = \phi\rho_f + (1-\phi)\rho_s$ is the mixture density, ϕ is the porosity; $\boldsymbol{s}$ is Voigt's representation of the stress tensor $\boldsymbol{\sigma}(\boldsymbol{x}, t)$: $\boldsymbol{s} = \{\sigma_{11}, \sigma_{22}, \sigma_{12}\}^T$; $p(\boldsymbol{x}, t)$ is the interstitial fluid pressure in the pores; the vectors of displacement of the solid skeleton and of the fluid are denoted by $\boldsymbol{u}^s(\boldsymbol{x}, t)$ and $\boldsymbol{u}^f(\boldsymbol{x}, t)$, respectively; the vector of relative displacement between the fluid and the solid frame weighted by the porosity is denoted by $\boldsymbol{w} = \phi(\boldsymbol{u}^f - \boldsymbol{u}^s)$; the tensor $\boldsymbol{k}$ is the anisotropic permeability tensor ($\boldsymbol{k} = \boldsymbol{\kappa}/\eta$ where $\boldsymbol{\kappa}$ is the intrinsic permeability tensor and η is the viscosity of the fluid) and the tensor $\boldsymbol{b}$ is defined as $\boldsymbol{b} = (\rho_f/\phi)\, \boldsymbol{a}$ with $\boldsymbol{a}$ is the tortuosity tensor; $\boldsymbol{m} = \{1, 1, 0\}^T$ and the operator $\mathbb{L}$ is defined as follows:

$$\mathbb{L} = \mathbf{L}_1\partial_1 + \mathbf{L}_2\partial_2,\ \mathbf{L}_1 = \begin{bmatrix} 1 & 0 \\ 0 & 0 \\ 0 & 1 \end{bmatrix},\ \mathbf{L}_2 = \begin{bmatrix} 0 & 0 \\ 0 & 1 \\ 1 & 0 \end{bmatrix}, \qquad (5)$$

where ∂_1 and ∂_2 denote the partial differentiation operators with respect to x_1 and x_2, respectively.

The constitutive equations for the anisotropic linear poroelastic material are given by:

$$\boldsymbol{s} = \mathbf{C}\, \boldsymbol{e} - \check{\boldsymbol{\alpha}}\, p, \quad p = -M\left(\boldsymbol{m}^T \mathbb{L}\boldsymbol{w} + \check{\boldsymbol{\alpha}}^T \mathbb{L}\boldsymbol{u}^s\right), \qquad (6)$$

where $\boldsymbol{e}$, $\mathbf{C}$, $\check{\boldsymbol{\alpha}}$ are Voigt's representation of the strain tensor $\boldsymbol{\epsilon}$, of the drained elastic tensor and of the Biot's effective tensor $\boldsymbol{\alpha}$, respectively: $\boldsymbol{e} = \{\epsilon_{11}, \epsilon_{22}, 2\epsilon_{12}\}^T$ and $\check{\boldsymbol{\alpha}} = \{\alpha_{11}, \alpha_{22}, \alpha_{12}\}^T$ (the superscript $\star^T$ designates the transpose operator); M is the Biot scalar modulus. By noting that $\boldsymbol{e} = \mathbb{L}\,\boldsymbol{u}$ and by using Eq. (6), one has:

$$\boldsymbol{s} = \mathbf{C}_u\, \mathbb{L}\, \boldsymbol{u}^s + \mathbf{C}_\alpha\, \mathbb{L}\, \boldsymbol{w}, \quad \boldsymbol{m}p = -\left(\mathbf{C}_M \mathbb{L}\boldsymbol{w} + \mathbf{C}_\alpha^T \boldsymbol{u}^s\right), \qquad (7)$$

where the quantities $\mathbf{C}_u, \mathbf{C}_\alpha$ and $\mathbf{C}_M$ are defined as: $\mathbf{C}_u = \mathbf{C} + M\check{\boldsymbol{\alpha}}\check{\boldsymbol{\alpha}}^T$, $\mathbf{C}_\alpha = M\check{\boldsymbol{\alpha}}\boldsymbol{m}^T$, $\mathbf{C}_M = M\boldsymbol{m}\boldsymbol{m}^T$. The tensor $\mathbf{C}_u$ is called the undrained elasticity tensor which may be considered as the rigidity of an equivalent elastic medium in which the relative movement between the interstitial fluid and solid skeleton is null (*i.e.* when $\boldsymbol{w} = \mathbf{0}$).

Boundary conditions At both interfaces Γ_1^{bf} and Γ_2^{bf}, the continuity of pressure and stress fields between the porous medium and the fluid domains is required. In addition, open-pore condition at the interfaces is assumed, requiring:

$$\left.\begin{array}{l} \dfrac{1}{\rho_j}\,\partial_2 p_j = -(\ddot{u}_2 + \ddot{w}_2) \\ p = p_j, \quad \boldsymbol{t} = \{0, -p_j\}^T \end{array}\right\}, \quad \forall \boldsymbol{x} \in \Gamma_j^{bf}, \qquad (8)$$

$$p_j \to 0, \quad \forall \boldsymbol{x} \to \Gamma_j^{f\infty}, \quad (j = 1, 2). \qquad (9)$$

where $\boldsymbol{u}^s = \{u_1, u_2\}^T$ and $\boldsymbol{w} = \{w_1, w_2\}^T$; the traction vectors $\boldsymbol{t}$ at the interfaces are defined by $\boldsymbol{t} = \mathbf{L}_2^T \boldsymbol{s} = \{\sigma_{21}, \sigma_{22}\}^T$.

3 Numerical method

The boundary value problem given by (Eqs. 1,2,3, refeq:elasdyn02a,8,9) deals with solving a system of linear partial differential equations of which the coefficients are constant with respect to x_1. Here we propose to solve the system as follows: (i) the system of equations is firstly transformed into wavenumber-frequency domain by using a Fourier transform with respect to x_1 combining to a Laplace transform with respect to t; (ii) in the wavenumber-frequency domain, the equations in both fluid domains are analytically solved giving impedance boundary conditions for the solid layer of which the dynamic equations will be solved by the finite element method; (iii) the space-time solution is finally obtained by performing two inverse transforms.

3.1 Equations in the Laplace-Fourier domain

We recall the general form of a Laplace-Fourier transform applied to a real-valued function $y(x_1, x_2, t)$: $\tilde{y}(k_1, x_2, s) := \int_0^\infty \left(\int_{-\infty}^{+\infty} y(x_1, x_2, t) e^{-ik_1 x_1} dx_1\right) e^{-st} dt$, where $i = \sqrt{-1}$; $s \in \mathbb{C}$ and $k_1 \in \mathbb{R}$; $\mathbb{R}$ and $\mathbb{C}$ denote the set of all the real and complex numbers, respectively.

Transformed problem in $(s-k_1)$ domain for the fluids Ω_1^f and Ω_2^f By applying the Laplace-Fourier transform to Eqs. (1,8, and 9), one obtains a differential equation for $\tilde{p}_1$ with respect only to x_2:

$$\left(\frac{s^2}{c_1^2}+k_1^2\right)\tilde{p}_1-\partial_2\tilde{p}_1=\rho_1\tilde{F}_0(s)\delta(x_2-x_2^s),\ \forall x_2>0, \quad (10)$$

$$\partial_2\tilde{p}_1=-\rho_1 s^2(\tilde{u}_2+\tilde{w}_2),\ \text{at } x_2=0, \quad (11)$$

$$\tilde{p}_2\to 0,\ \text{for } x_2\to+\infty. \quad (12)$$

The solution of this system may be presented in a semi-explicit form as follows:

$$\tilde{p}_1=-\frac{\rho_1\tilde{F}_0}{2\beta_1}\left(e^{-\beta_1(x_2^s-x_2)}+e^{-\beta_1(x_2^s+x_2)}\right)+\frac{\rho_1 s^2\tilde{G}_{21}}{\beta_1}e^{-\beta_1 x_2},\quad \forall\ 0\le x_2\le x_2^s \quad (13)$$

$$\tilde{p}_1=-\frac{\rho_1\tilde{F}_0}{2\beta_1}\left(e^{\beta_1(x_2^s-x_2)}+e^{-\beta_1(x_2^s+x_2)}\right)+\frac{\rho_1 s^2\tilde{G}_{21}}{\beta_1}e^{-\beta_1 x_2},\quad \forall\ x_2\ge x_2^s \quad (14)$$

where $\beta_1=\sqrt{\frac{s^2}{c_1^2}+k_1^2}$ and $\tilde{G}_{21}=\tilde{u}_2(k_1,0,s)+\tilde{w}_2(k_1,0,s)$.

Similarly, the solution of $\tilde{p}_2$ in $(s-k_1)$ domain may be expressed as follows:

$$\tilde{p}_2=-\frac{\rho_2 s^2\tilde{G}_{22}}{\beta_2}e^{\beta_2(x_2+h)},\qquad \forall x_2\le -h, \quad (15)$$

where $\beta_2=\sqrt{\frac{s^2}{c_2^2}+k_1^2}$ and $\tilde{G}_{22}=\tilde{u}_2(k_1,-h,s)+\tilde{w}_2(k_1,-h,s)$

3.2 Transformed problem in $(s-k_1)$ domain for the solid Ω^b

By noting that in the Fourier-Laplace domain the operator $\mathbb{L}$ becomes $\tilde{\mathbb{L}}=ik_1\mathbf{L}_1+\partial_2\mathbf{L}_2$, the boundary value problem defined by Eqs. (3) and (4) may be transformed into the $(s-k_1)$ domain as follows:

$$\rho s^2\tilde{\boldsymbol{u}}^s+\rho_f s^2\tilde{\boldsymbol{w}}-ik_1\mathbf{L}_1^T\tilde{\boldsymbol{s}}-\partial_2\mathbf{L}_2^T\tilde{\boldsymbol{s}}=\mathbf{0} \quad (16)$$

$$\rho_f s^2\tilde{\boldsymbol{u}}^s+\left(s\boldsymbol{k}^{-1}+s^2\boldsymbol{b}\right)\tilde{\boldsymbol{w}}+ik_1\mathbf{L}_1^T\boldsymbol{m}\tilde{p}+\mathbf{L}_2^T\partial_2(\boldsymbol{m}\tilde{p})=\mathbf{0} \quad (17)$$

where the constitutive equations (see Eq. (7)) read:

$$\begin{aligned}\tilde{\boldsymbol{s}}&=ik_1(\mathbf{C}_u\mathbf{L}_1\tilde{\boldsymbol{u}}^s+\mathbf{C}_\alpha\mathbf{L}_1\tilde{\boldsymbol{w}})+\mathbf{C}_u\mathbf{L}_2\partial_2\tilde{\boldsymbol{u}}^s+\mathbf{C}_\alpha\mathbf{L}_2\partial_2\tilde{\boldsymbol{w}},\\ -\boldsymbol{m}\tilde{p}&=ik_1(\mathbf{C}_\alpha^T\mathbf{L}_1\tilde{\boldsymbol{u}}^s+\mathbf{C}_M\mathbf{L}_1\tilde{\boldsymbol{w}})+\mathbf{C}_\alpha^T\mathbf{L}_2\partial_2\tilde{\boldsymbol{u}}^s+\mathbf{C}_M\mathbf{L}_2\partial_2\tilde{\boldsymbol{w}}.\end{aligned} \quad (18)$$

By replacing (18) into Eqs. (16)-(17) and then making some arrangements, we obtain a vectorial form of this problem:

$$s^2\mathbb{A}_1\mathbb{v}+s\mathbb{A}_2\mathbb{v}+k_1^2\mathbb{A}_3\mathbb{v}-ik_1\mathbb{A}_4\partial_2\mathbb{v}-\partial_2\mathbb{t}=\mathbb{O}, \quad (19)$$

where $\mathbb{v}=\left(\tilde{\boldsymbol{u}}^s,\tilde{\boldsymbol{w}}\right)^T$, $\mathbb{t}=ik_1\mathbb{A}_4^T\mathbb{v}+\mathbb{A}_5\partial_2\mathbb{v}$ and

$$\mathbb{A}_1=\begin{bmatrix}\rho\mathbf{1} & \rho_f\mathbf{1}\\ \rho_f\mathbf{1} & \boldsymbol{b}\end{bmatrix},\ \mathbb{A}_2=\begin{bmatrix}\mathbf{0} & \mathbf{0}\\ \mathbf{0} & \boldsymbol{k}^{-1}\end{bmatrix},\ \mathbb{A}_3=\begin{bmatrix}\mathbf{C}_u^{11} & \mathbf{C}_\alpha^{11}\\ \left(\mathbf{C}_\alpha^{11}\right)^T & \mathbf{C}_M^{11}\end{bmatrix},$$
$$\mathbb{A}_4=\begin{bmatrix}\mathbf{C}_u^{12} & \mathbf{C}_\alpha^{12}\\ \left(\mathbf{C}_\alpha^{21}\right)^T & \mathbf{C}_M^{12}\end{bmatrix},\ \mathbb{A}_5=\begin{bmatrix}\mathbf{C}_u^{22} & \mathbf{C}_\alpha^{22}\\ \left(\mathbf{C}_\alpha^{22}\right)^T & \mathbf{C}_M^{22}\end{bmatrix}. \quad (20)$$

In later equations, the 2-by-2 matrices $\mathbf{C}_u^{ab}$, $\mathbf{C}_\alpha^{ab}$ and $\mathbf{C}_M^{ab}$ with $a,b=1,2$ are defined by:

$$\mathbf{C}_u^{ab}=\mathbf{L}_a^T\mathbf{C}_u\mathbf{L}_b,\ \mathbf{C}_\alpha^{ab}=\mathbf{L}_a^T\mathbf{C}_\alpha\mathbf{L}_b,\ \mathbf{C}_M^{ab}=\mathbf{L}_a^T\mathbf{C}_M\mathbf{L}_b. \quad (21)$$

The 4-by-4 matrices $\mathbb{A}_1,\mathbb{A}_2,\mathbb{A}_3,\mathbb{A}_4$ and $\mathbb{A}_5$ depend only on the material properties of the elastic porous material.

At two interfaces $x_2=0$ and $x_2=-h$, in view of Eqs. (13)-(15), the continuity conditions (8) between fluid pressures and stress traction require that:

$$\mathbb{t}(0)=-\mathbf{P}_1\,\mathbb{v}(0)+\mathbf{F}_0,\quad \mathbb{t}(-h)=\mathbf{P}_2\,\mathbb{v}(-h), \quad (22)$$

where

$$\mathbf{P}_1=\frac{\rho_1 s^2}{\beta_1}\mathbf{P},\quad \mathbf{P}_2=\frac{\rho_2 s^2}{\beta_2}\mathbf{P},\quad \mathbf{P}=\begin{bmatrix}0&0&0&0\\0&1&0&1\\0&0&0&0\\0&1&0&1\end{bmatrix}, \quad (23)$$

$$\mathbf{F}_0=\left\{0,\ \tfrac{\rho_1\tilde{F}_0}{\beta_1}e^{-\beta_1 x_2^s},\ 0,\ \tfrac{\rho_1\tilde{F}_0}{\beta_1}e^{-\beta_1 x_2^s}\right\}^T. \quad (24)$$

3.3 Finite element formulation in spectral domain and time-space solution

Weak formulation The weak formulation of the boundary value problem given by (19) and (22) may be now performed. Let $\mathscr{C}^{ad}$ be the admissible function space of the problem constituted by the sufficiently differentiable complex-valued functions such as: $x_2\in H^b=]-h,0[\to\delta\mathbb{v}(x_2)\in\mathbb{C}^4$. Upon integrating (19) against a test vector function $\delta\mathbb{v}$ and integrating by part, then applying the boundary condition (22), the weak formulation of Eq. (19) reads:

$$\begin{aligned}&s^2\langle\,\delta\mathbb{v},\mathbb{A}_1\mathbb{v}\,\rangle_{H^b}+s\langle\,\delta\mathbb{v},\mathbb{A}_2\mathbb{v}\,\rangle_{H^b}+k_1^2\langle\,\delta\mathbb{v},\mathbb{A}_3\mathbb{v}\,\rangle_{H^b}\\&+ik_1\left\{\left\langle\,\partial_2\delta\mathbb{v},\mathbb{A}_4^T\mathbb{v}\,\right\rangle_{H^b}-\langle\,\delta\mathbb{v},\mathbb{A}_4\partial_2\mathbb{v}\,\rangle_{H^b}\right\}\\&+\langle\,\partial_2\delta\mathbb{v},\mathbb{A}_5\partial_2\mathbb{v}\,\rangle_{H^b}+\delta\mathbb{v}^*(0)\,\mathbf{P}_1\mathbb{v}(0)\\&+\delta\mathbb{v}^*(-h)\,\mathbf{P}_2\mathbb{v}(-h)=\delta\mathbb{v}^*(0)\,\mathbf{F}_0,\quad\forall\,\delta\mathbb{v}\in\mathscr{C}^{ad},\end{aligned} \quad (25)$$

where $\langle .,.\rangle_{H^b}$ denotes the inner product over H^b; $\delta\mathbb{v}^*$ is the conjugate transpose of $\delta\mathbb{v}$.

Finite element formulation We proceed by introducing a finite element mesh of the domain $[-h,0]$ which contains n^{el} elements: $[-h,0]=\bigcup_e\Omega_e$ with $e=1,...,n^{el}$. By using the Galerkin finite element method, for which both functions $\mathbb{v}$ and $\delta\mathbb{v}$ in each element Ω_e are approximated using the same shape function $\mathbf{N}_e$, one may derive the finite element equation in the following form:

$$\left(s^2\mathbf{K}_1+s\mathbf{K}_2+k_1^2\mathbf{K}_3+ik_1\mathbf{K}_4+\mathbf{K}_5+\mathbf{K}^\Gamma\right)\mathbf{V}=\mathbf{F}, \quad (26)$$

where $\mathbf{V}$ is the global nodal solution vector; the vector $\mathbf{F}$ is the external force vector due to the acoustical source; $\mathbf{K}^\Gamma$ represents the coupled operator between the fluid and poroelastic layers; $\mathbf{K}_j$ ($j=1..5$) are the global matrices of the poroelastic layer (see [15] for further details)

Computation of time-space solution For fixed values of (s,k_1) in the Laplace-Fourier transformed domain, the solution of $\mathbb{v}$ may be computed by solving the system of complex linear equations (26). The solutions for $\tilde{p}_1$ and $\tilde{p}_2$ in two fluid domains may then be determined by using the equations (13)-(14) and (15), respectively.

In order to obtain the spatio-temporal solution, we need to perform a numerical inverse Laplace-Fourier transform. In this paper, the inverse Fourier transform is computed by using the usual FFT (Fast Fourier Transform) technique. The

inverse Laplace transform is carried out using the Quadrature Convolution Method which has proved to be a very efficient technique for computing the time response solution in many dynamic problems [17].

4 Results

Physical parameters This section presents some numerical tests describing an *in vivo* ultrasound test on human cortical long bones. The acoustic source (Eq. 1) located at the position $(x_1^s, x_2^s) = (0, 2)$ (in mm) in the upper fluid domain Ω_1^f has the time-history function given by: $F(t) = F_0\, e^{-4(f_c t-1)^2} \sin(2\pi f_c t)$, where $F_0 = 1\,\mathrm{m.s^{-2}}$ and $f_c = 1$ MHz which is the central frequency. The spectrum frequency bandwidth of this signal is about 0 – 2.5 MHz.

Both fluid domains Ω_1^f and Ω_2^f are assumed to be identical and are considered as an idealized water. The mechanical properties of the fluids are given by $\rho_1 = \rho_2 = 1\,000\ \mathrm{kg.m^{-3}}$ et $K_1 = K_2 = 2.25$ GPa. Thus the wave velocities in two fluid domains are: $c_1 = c_2 = 1\,500\ \mathrm{m.s^{-1}}$.

In order to describe the behavior of the poroelastic bone plate, the drained elasticity tensor $\boldsymbol{C}$ as well as Biot's effective coefficients $\check{\boldsymbol{\alpha}}$ and M used in Eq. (6) should be provided. For this study, these parameters are derived from the characteristics of the interstitial fluid and solid skeleton phases by using a continuum micromechanics model proposed by Hellmich *et al* [18].

For the numerical tests presented here, the interstitial fluid is also assumed to be the same as the exterior fluid domain, *i.e.* $\rho_f = 1\,000\ \mathrm{kg.m^{-3}}$ et $K_f = 2.25$ GPa. The solid bone has the mass density $\rho_s = 1\,722\ \mathrm{kg.m^{-3}}$ and is assumed to be a transversely isotropic elastic material [18]. The components of the elastic tensor of the solid phase are given by using the Voigt's notations: $c_{11}^m = 28.7$ GPa, $c_{22}^m = 23.6$ GPa, $c_{12}^m = 9.9$ GPa, $c_{66}^m = 7.25$ GPa, $c_{16}^m = c_{26}^m = 0$. The viscosity of interstitial fluid is $\eta = 1 \times 10^{-3}$ Pa.s and the permeability tensor is roughly taken by $\kappa_{11} = \kappa_{22} = 5 \times 10^{-13}\ \mathrm{m^2}$ [6].

Validation We consider a bone layer which has a porosity $\phi = 0.05$ and a constant thickness $h = 4$ mm. The numerical parameters used for simulation have been chosen in a similar way to which required for a classical procedure of dynamic finite element analysis [9]. The space interval Δx is about the $1/10$ shortest wavelength. The time step is chosen for satisfying the CFL condition. Here, the space interval in $\mathbf{e}_1$-direction has been chosen to be $\Delta x = 0.75 \times 10^{-4}\ m$. The time step used is $\Delta t = 10^{-7} s$. To perform the finite element analysis on vertical direction $\mathbf{e}_2$, the bone plate's thickness is discretized into 12 quadratic Lagrangian elements.

Figure 2 presents snapshots of the wave field in the coupled trilayer system at the instants $t = 5\ \mu$s. At each point $\boldsymbol{x}$ in the domain, the quantity presented for obtaining these snapshots is $\log(|p_1(\boldsymbol{x}, t)|)$ if $\boldsymbol{x} \in \Omega_1^f$, $\log(|p_2(\boldsymbol{x}, t)|)$ if $\boldsymbol{x} \in \Omega_2^f$ and $\log(|p(\boldsymbol{x}, t)|)$ if $\boldsymbol{x} \in \Omega^b$. In this figure, we can clearly observe the transmission and reflection of ultrasonic waves through the interfaces. Note that using the proposed method allows us to take into account the exact radiation conditions of two fluid domains, therefore the results involve only the waves diffracted by the bone layer.

Figure 3 presents the numerical solution of p_1 measured at two positions $\mathrm{R}_1(x_1, x_2) = (2, 2)$ (mm) (upper) and

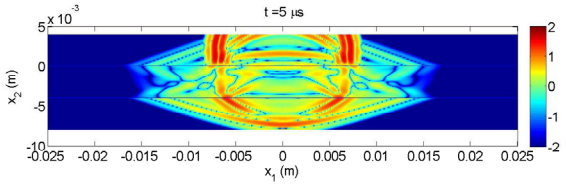

Figure 2: Snapshots of the fluid pressure (p_1, p and p_2)

$\mathrm{R}(x_1, x_2) = (20, 2)$ (mm) (lower) by using the proposed spectral/finite element procedure. We also present numerical solutions obtained by using conventional time domain finite element analysis [9]. The comparison shows that proposed semi-analytical/FE and conventional FEM results perfectly match each to other. Note that both methods use the same time step for the calculation. Due to the fact that only very small matrices need to be factorized, the proposed method only requires 400 seconds to obtain these results by using a very common PC.

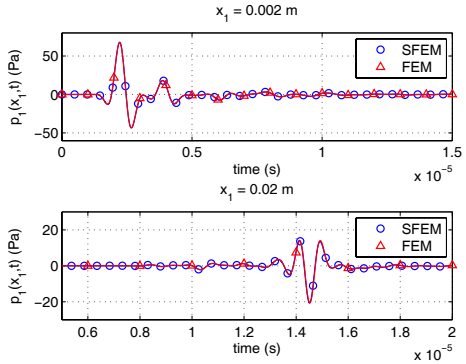

Figure 3: Comparison between SFE and FE solutions of p_1 at $x_1 = 2$ mm (upper) and at $x_1 = 20$ mm (lower)

Influence of porosity on FAS velocity When the axial transmission technique is used, the FAS First Arriving Signal velocity have been shown to be a relevant index of bone status . In this section, we aim to study the influence of the bone's porosity on the FAS velocity denoted by V_F. For this purpose, the material properties of bone matrix $(\rho_m, \boldsymbol{c}_m)$ were fixed. The poroelastic properties were then determined by using the micromechanics analysis. The FAS velocity is determined V_F based first zero-crossing locations on time axis of measured p_1-signal captured at an array of 14 sensors which has a gap 0.8 mm from each to other.

Figure 4 shows the variation of the FAS velocity with respect to ϕ when considering a bone plate with thickness $h = 4$ mm. One may observe that the V_F *versus* ϕ relation is practically linear and V_F decreases when the porosity ϕ is higher. We also present in this graph the V_F *versus* ϕ relation obtained by using equivalent elastic media. For a given porosity ϕ, the corresponding elastic models use the mass density taken as the mixture density and the elasticity tensor is taken as the undrained elasticity tensor $\boldsymbol{C}_u$ (Eq. (7)). For lower porosities, the V_F obtained by using the poroelastic model are slightly different from the ones obtained using the elastic model. The difference becomes more significant for higher porosity because the fluid-solid movement is

more important and would be not negligible. A similar discussion may be made when considering a thin bone layer (h = 0.6 mm) (see more detail in [19]).

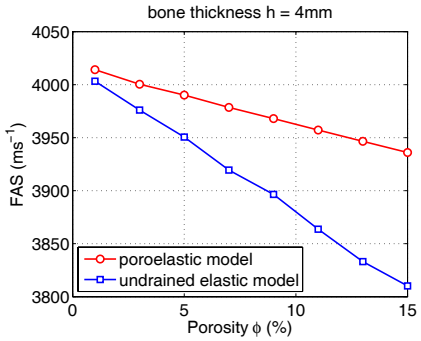

Figure 4: FAS velocities *versus* different bone porosities

5 Conclusion

By using a hybrid semi-analytical/finite element technique, we have derived a finite element formulation in spectral domain for anisotropic poroelastic plate saturated by an interstitial fluid and immersed in a fluid. The procedure is based on a Laplace-Fourier transform which leads to a one-dimensional differential equation with respect only to x_2 which may be solved by using conventional FEM. In the Laplace-Fourier domain, the radiation conditions presenting two half-spaces of fluid may exactly be introduced. Since only one-dimensional finite element problem need to be solved in spectral domain, the proposed procedure requires a very small memory size for computation. In addition, the computation time is very low, especially for the configuration used for ultrasonic test presented here wherein we only need to compute the time-domain solution at some specific points.

Using the proposed method, numerical studies of ultrasonic wave propagation in poroelastic bone layer may be easily carried out, eventually in the very high frequency domain. This allows us to consider the anisotropy and the heterogeneity of the bone matrix material as well as bone porosity. Some preliminary results presented in this paper show that the FAS velocity is strongly influenced by the bone porosity. It seems that using of equivalent elastic model might lead to a poor estimation of FAS velocity in cortical bone with higher bone porosity.

References

[1] Lowet G, Van der Perre G. Ultrasound velocity measurements in long bones: measurement method and simulation of ultrasound wave propagation. *J. Biomech.* 1996; **29**:1255–1262.

[2] Dong NX, Guo EX. The dependence of transverse isotropic elasticity of human femoral cortical boneon porosity. *J. Biomech.* 2004; **37**(8):1281–1287.

[3] Baron C, Naili S. Propagation of elastic waves in a fluid-loaded anisotropic functionally graded waveguide: Application to ultrasound characterization. *J. Acoust. Soc. Am* 2010; **127**(3):1307–1317.

[4] Bossy E, Talmant M, Laugier P. Effect of bone cortical thickness on velocity measurements using ultrasonic axial transmission: A 2D simulation study. *J. Acoust. Soc. Am.* 2002; **112**:297–307.

[5] Desceliers C, Soize C, Grimal Q, Haiat G, Naili S. A time-domain method to solve transient elastic wave propagation in a multilayer medium with a hybrid spectral-finite element space approximation. *Wave Motion* 2008; **45**(4):383 – 399.

[6] Cowin SC. Bone poroelasticity. *J. Biomech.* 1999; **32**:217–238.

[7] Nguyen VH, Lemaire T, Naili S. Poroelastic behaviour of cortical bone under harmonic axial loading: A finite element study at the osteonal scale. *Med. Eng. & Phys.* 2010; **32**(4):384 – 390.

[8] Williams JL. Ultrasonic wave propagation in cancellous and cortical bone: prediction of some experimental results by Biot's theory. *J. Acoust. Soc. Am.* 1992; **91**(2):1106–1112.

[9] Nguyen VH, Naili S, Sansalone V. Simulation of ultrasonic wave propagation in anisotropic cancellous bones immersed in fluid. *Wave Motion* 2010; **47**(2):117–129.

[10] Kausel E. *Fundamental Solution in Elastodynamics*. Cambridge University Press, 2006.

[11] Protopappas VC, Kourtis IC, Kourtis LC, *et al*. Three-dimensional finite element modeling of guided ultrasound wave propagation in intact and healing long bones. *J. Acoust. Soc. Am.* 2007; **121**(6):3907–3921.

[12] Liu G, Xi ZC. *Elastic Waves in Anisotropic Laminates*. CRC Press, 2002.

[13] Gopalakrishnan S, Chakraborty A, Roy Mahapatra D. *Spectral Finite Element Method*. Spinger, 2008.

[14] Marzani A. Time-transient response for ultrasonic guided waves propagating in damped cylinders. *Int. J. Solids Struct.* 2008; **45**(25-26):6347 – 6368.

[15] Nguyen VH, Naili S, Ultrasonic wave propagation in viscoelastic cortical bone plate coupled with fluids: A spectral finite element study. *Comput. Meth. Biomech. Biomed. Eng.*, 2012 (in press)

[16] Cheng AH. Material coefficients of anisotropic poroelasticity. *Int. J. Rock Mech. and Min. Sci.* 1997; **34**(2):199–205.

[17] Schanz M, Antes H. Application of 'Operational Quadrature Methods' in time domain boundary element methods. *Meccanica* 1997; **32**:179–186.

[18] Hellmich C, Ulm FJ. Microporodynamics of bones: Prediction of the "Frenkel-Biot" slow compressional wave. *J. Engrg. Mech.* 2005; **131**(9):918–927.

[19] Nguyen VH, Naili S, Simulation of ultrasonic wave propagation in anisotropic poroelastic bone plate using spectral finite element method. *Int. J. Num. Meth. Biomed. Eng.*, 2012 (in press).